J Mater Sci (2011) 46:4540–4544
DOI 10.1007/s10853-011-5348-4

In situ study on the formation of FeTe

J.-C. Grivel · A. C. Wulff · Y. Zhao · J. Bednarčík · M. v. Zimmermann

Received: 17 November 2010 / Accepted: 29 January 2011 / Published online: 15 February 2011

Abstract The formation of the FeTe compound from a mixture of Fe and Te powders was studied in situ by means of high-energy synchrotron X-ray diffraction. FeTe does not form directly from the starting elements; instead, $FeTe_2$ forms as an intermediate product. During a 2 °C/min heating ramp, Te first reacts between 200 and 350 °C with a part of the Fe powder to form $FeTe_2$, which then further reacts between 350 and 530 °C with the remaining Fe to yield FeTe. This phase formation path is simpler than in the case of FeSe and the differences are discussed in terms of the equilibrium phase diagrams of these two systems.

Introduction

The FeTe compound crystallises in the tetragonal P4/nmm structure [1] similar to that of FeSe [2]. Both consist of layers of edge-sharing tetrahedra, $FeTe_4$ and $FeSe_4$, respectively, arranged according to the tetragonal PbO type with Fe atoms in the oxygen positions and Te or Se in the Pb positions [1]. FeTe exhibits a semiconducting behaviour [3], but can be turned to a superconductor by doping with either Se [4, 5] or S [6], in the latter case with a clear enhancement effect through exposure to water vapour [7]. Although, the superconducting transition temperatures of these compounds are not especially elevated (for instance, it reaches about 15 K in $FeSe_{0.5}Te_{0.5}$ [8]), they are characterised by very high upper critical fields $H_{c2}(0)$ reaching up to more than 100 T [9], which makes them potentially interesting for technological applications. Owing to the possibility of processing this material at relatively low temperatures and the lower toxicity of the starting reagents in comparison with FeAs-based superconductors, compounds in the Fe–Te–Se–S system could be interesting for power devices and electromagnets applications if high-critical current density (j_c) wires can be developed. For this purpose, preliminary attempts to manufacture Fe(Se,Te) wires using a diffusion technology, in which a Se–Te precursor powder was loaded into a Fe tube that acted as a Fe source for the formation of a Fe(Se,Te) diffusion layer were recently reported by Mizuguchi et al. [10]. Unfortunately, the critical current densities of the wires after processing were limited to low values in the 10–100 A/cm^2 range at 4.2 K. The microstucture of the superconducting core of the wires was characterised by extended porosity and it is apparent that their performance was limited by defects. Improving the critical current density of Fe(Te,Se,S)-based wires clearly necessitates a sound understanding of the formation mechanism of these superconductors from the starting reagents. In a recent study, the authors investigated the reactions taking place during the synthesis of the structurally similar FeSe phase and found that its formation from a mixture of Fe and Se powders involves three intermediate binary compounds appearing in the $FeSe_2$, Fe_3Se_4, Fe_7Se_8 sequence [1]. Prior to studying the formation of the $FeSe_{1-x}Te_x$ or $FeTe_{1-x}S_x$ compounds, the authors focus on the formation of the FeTe phase from a mixture of Fe and Te powders in order to gain knowledge on the behaviour of this simpler system. The Fe–Te phase diagram [12–15] departs

J.-C. Grivel (✉) · A. C. Wulff · Y. Zhao
Materials Research Division, Risø National Laboratory for Sustainable Energy, Technical University of Denmark, Frederiksborgvej 399, 4000 Roskilde, Denmark
e-mail: jean@risoe.dtu.dk

J. Bednarčík · M. v. Zimmermann
Hamburger Synchrotronstrahlungslabor, HASYLAB at Deutsches Elektronen-Synchrotron DESY, Notkestrasse 85, 22603 Hamburg, Germany

significantly from the Fe–Se phase diagram [16] so that this study will give hints about the more complicated Fe–Se–Te and Fe–Te–S systems, the phase equilibria of which are yet unknown. Since the melting temperature of Te is only slightly higher than that of Se (450 versus 221 °C) and both Te and FeTe have a relatively high vapour pressure in the temperature range used during this study [17, 18], the authors used the same approach as for the study of the FeSe phase formation [11] i.e., in situ reaction studies were conducted on a powder mixture encased into a composite Cu/Nb protective metal sheath taking advantage of the strong penetrating power of high-energy synchrotron X-ray radiation and thus avoiding Te losses by evaporation.

Experimental details

The starting reagents: Fe powder (99.9% purity, <10 μm) and Te powder (99.99%, −325 mesh) were mixed in a Fe : Te = 1.0:0.9 atomic ratio by low-energy ball milling in 4 cm diameter polyethylene jars for 24 h with NiO balls (5 pieces of 4 g for 5 g powder) using a Wheaton roller mill at 50 rpm rotation speed. The choice of this Te-deficient stoichiometry, equivalent to $Fe_{0.53}Te_{0.47}$ is based on the published determinations of the $Fe_{1+x}Te_{1-x}$ solid solution range [13–15, 19]. The mixed powder was packed in a Nb tube (external diameter 5 mm, wall thickness 0.3 mm), which was then deformed by groove rolling into a wire with 4.0 mm diameter. At this stage, the wire was inserted into a Cu tube (external diameter 5 mm, wall thickness 0.5 mm) and the Cu/Nb/(Fe–Te) composite was further deformed by means of groove rolling into a wire with an approximately square cross section of 1.75 × 1.75 mm^2.

The in situ measurements were conducted at the high energy X-ray beamline BW5, located at the storage ring DORIS III at DESY. The photon energy of the incident beam was 80 keV. Details on the experimental set-up and data analysis can be found in a previous publication [20]. A short sample piece (≅4 cm length) cut from the wire was clamped in a high-temperature steel holder inserted in a quartz tube. The sample holder assembly was placed in a high-temperature furnace equipped with Kapton windows and a stainless steel heat shield with holes for beam entrance and exit. The sample was maintained in a flow of Ar (≤0.5 ppm residual O_2) during the runs. A heating rate of 2 °C/min was used to reach a maximum temperature of 584 °C, at which the sample was maintained for 1 h. A thermometer was situated close to the sample and the temperature was stable within 1 °C during the 1 h long dwell at 584 °C. Cooling was performed at 5 °C/min. The acquisition time was 2 s for each diffraction pattern.

A beam cross-section of 1 × 1 mm^2 was chosen to probe the ceramic core throughout the diameter of the wire. Absorption scans were used to position the sample in the beam. Diffraction patterns were recorded on a two-dimensional image plate and evaluated using the fit2d software package [21]. The intensity of the signal was normalised to the synchrotron positron beam current value, which varies with time during the experiment.

Scanning electron microscope (SEM) observations were performed in a Supra 35 instrument equipped with a Thermo Electron Corporation energy dispersive X-ray detector (EDX) for compositional analysis. For the SEM observations, transversal cross-sections of the wire that was used for the synchrotron experiment as well as a sample cut from the same wire but without heat treatment were cast in epoxy resin and polished using diamond paste.

Results and discussion

An optical micrograph of the cross-section of the piece cut from the wire before annealing is shown in Fig. 1. The Nb sheath forms a continuous protecting layer between the Cu external sheath and the Fe–Te powder mixture. This feature is essential to prevent the formation of a low-temperature eutectic liquid phase (340 °C) by contact between Cu and Te [22].

Selected XRD patterns recorded at various temperatures along the heating ramp are shown in Fig. 2. The $FeTe_2$ phase forms as an intermediate product during the transformation from the initial Fe and Te mixture into FeTe. Figure 3 depicts the temperature variation of the integrated intensity of selected, non-overlapping reflections for the different phases. It must be emphasized that the intensity scale in Fig. 3 does not provide absolute phase contents. However, it enables to follow the relative content variations of the observed compounds.

During heating from room temperature up to about 250 °C, the full width at half maximum of the Te

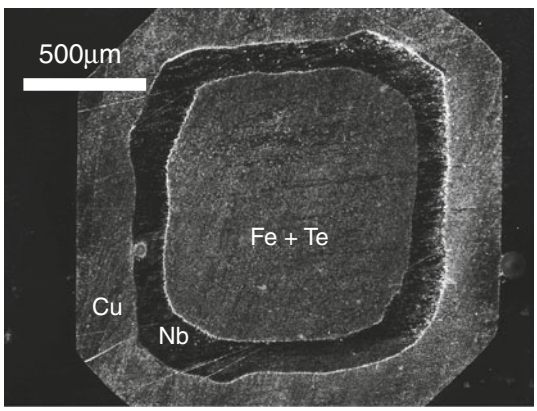

Fig. 1 General view (optical micrograph) of a transverse cross-section of a wire before annealing

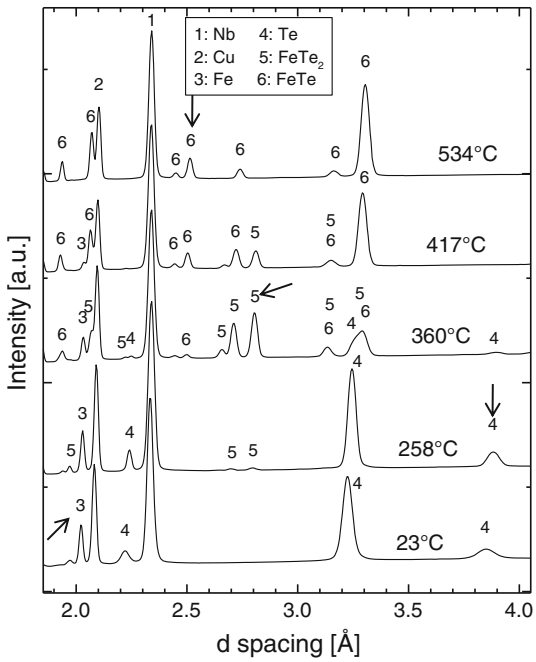

Fig. 2 Diffraction patterns collected at various temperatures during the heating ramp. The reflections used for intensity integration are indicated by *arrows*

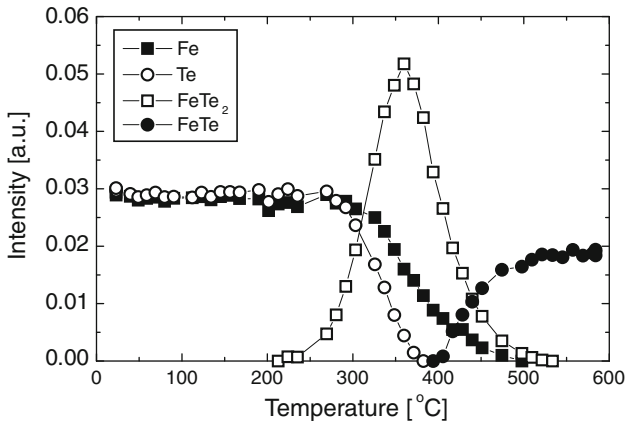

Fig. 3 Temperature dependence of the integrated intensity of selected diffraction peaks during heating at 2 °C/min: Fe(110), Te(100), $FeTe_2$(111) and FeTe (111)

diffraction peaks is decreasing. Release of the strain accumulated during mechanical deformation of the wire and/or grain growth can be reasons for this feature. As evidenced in Fig. 3, the starting mixture of Fe and Te begins to react in the solid state slightly above 200 °C with the formation of $FeTe_2$. This reaction is slow up to 250 °C but proceeds at a significantly faster rate between 250 and 350 °C. The volume fraction of this phase goes through a maximum at 355 °C and its amount then starts to decrease. The first traces of FeTe are detected around 400 °C and the intensity of this phase's diffraction peaks increases until saturation at a temperature corresponding to that of the disappearance of the $FeTe_2$ phase (about 530 °C). As expected from the formation of $FeTe_2$ in the wires, the intensity of the Fe lines start to decrease at the same temperature as those of Te. However, whereas Te has disappeared at 380 °C i.e., well below the melting point of pure Te, Fe is still present and can be detected up to 500 °C. At this point, the intensity of the $FeTe_2$ diffraction peaks is also vanishing and most of the FeTe phase has formed. From these observations, the authors can conclude that the FeTe phase does not form by direct reaction of the starting Fe and Te powders but following interaction between the $FeTe_2$ intermediate product and the remaining Fe. No further changes were detected during the 1 h dwell at 584 °C.

In Fig. 4 the microstructure of the Fe–Te core of the wire before and after heat treatment is compared. In the as-deformed state, Fe particles are embedded within a matrix consisting of Te. The largest Fe grains are still close to 10 μm in diameter, indicating that the mechanical deformation of the wire has not resulted in milling of these particles. In contrast, the size of the Te particles, which can only be distinguished close to holes formed in the core during polishing, is typically smaller than 1 μm. This is much smaller than the starting particle size (<325 mesh =

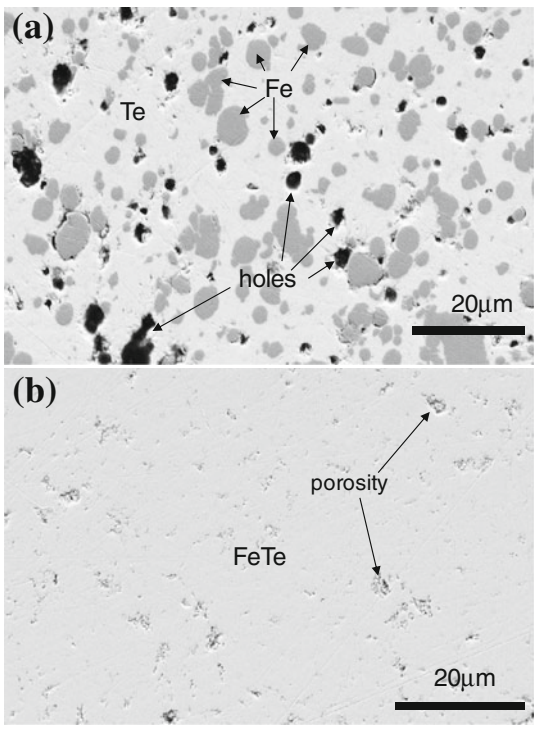

Fig. 4 SEM pictures (secondary electron images) showing details of the Fe–Te core: **a** before heat treatment and **b** after heat treatment at 584 °C for 1 h on polished transverse cross-sections of the samples used for the in situ synchrotron investigation

44 μm). The particle size of both starting powders and the powder mixture prior to packing in the metal tubes has been observed by microscopy. Many particles with size in excess of 10 μm and up to 40 μm were found as expected in the as-purchased Te powder, whereas the starting Fe powder is characterised by particles of 10 μm diameter or less. After ball milling, the powder mixture still contains large (>10 μm) particles, indicating that the low-energy milling used in the present process does not affect the particle size to a significant extent. The decrease in Te average particle size is thus mostly occurring during mechanical deformation of the composite metal/powder tube to a wire. These observations indicate that both components of the powder mixture deform in very different ways during the wire preparation process: the Te powder being prone to milling during deformation in contrast to Fe. Higher homogeneity of the starting mixture can therefore not been expected from mechanical milling of the Fe particles during wire deformation; instead, Fe powders with smaller particle size must be used. After heat treatment, the Fe particles have disappeared as expected from the X-ray diffraction data and the microstructure is characterised by a relatively high density with porous areas of a size smaller than that of the initial Fe particles. The overall porosity has not been changed significantly by the heat treatment and is lower than that resulting from the diffusion technique used by Mizuguchi et al. [10].

Pictures of the Nb/FeTe interface before and after the heat treatment are shown in Fig. 5. There is an intimate contact between the core and the Nb layer in the as-deformed state, but it is essentially lost after the reaction. A lack of interface contact might be a problem in view of current transfer between the metal sheath and the ceramic core. This issue is not a concern in the case of FeTe since this compound is not a superconductor but might become very important in the case of the related superconducting Fe(Se,Te) phases. A fine tuning of the processing parameters, in particular heat treatment may prove necessary to avoid this problem. Although some particles still stick onto the Nb, the authors could not find evidence for the formation of compounds including Nb and Fe or Te. Nb therefore appears to be effective as an inert sheath metal for FeTe-based wires as it is for FeSe [11] and $Sr_{0.6}K_{0.4}Fe_2As_2$ [23].

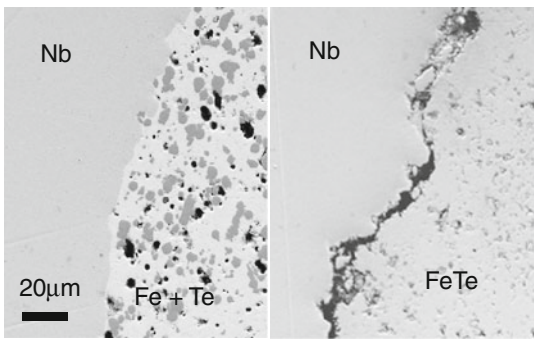

Fig. 5 Detail of the Nb–FeTe ceramic core interface: **a** before and **b** after heat treatment at 584 °C for 1 h (SEM, secondary electron image)

The reaction of Fe and Se powders to form the superconducting FeSe phase also begins with the formation of the $FeSe_2$ compound [11]. However, contrary to the case of FeTe, FeSe does not form by further direct reaction between $FeSe_2$ and Fe, but involves other intermediates with Fe_3Se_4 and Fe_7Se_8 composition. Beside FeTe and $FeTe_2$, the Fe–Te system also includes other Te-rich binary compounds with $FeTe_{1.5}$ (δ-phase) and $FeTe_{1.1}$ (γ-phase) approximate compositions, but these are only stable at temperatures in excess of 515 °C [1, 12–15], whereas Fe_3Se_4 and Fe_7Se_8 can form at much lower temperatures (these phases are stable from at least 200 °C according to the phase equilibria studies performed on the Fe–Se system [16]). Since the formation of FeTe was nearly complete at 515 °C in the sample during heating, the formation of $FeTe_{1.5}$ and $FeTe_{1.1}$ upon reaction between Fe and $FeTe_2$ was avoided. It is, however, not excluded that these phases may form as additional intermediates, if a faster heating rate is used in such a way that the FeTe phase formation is still far from being finished before the temperature of the system reaches the stability region of $FeTe_{1.5}$ and $FeTe_{1.1}$.

Conclusion

The formation of the FeTe phase from Fe and Te involves the formation of $FeTe_2$ as an intermediate product, which reacts with Fe to form FeTe. At the used heating rate of 2 °C/min, Te is consumed before the temperature of the system reaches the melting point of this element. The FeTe formation was complete at about 530 °C, thus preventing the occurrence of detectable amounts of $FeTe_{1.5}$ and/or $FeTe_{1.1}$ as additional intermediates.

Acknowledgements The authors gratefully acknowledge technical assistance from J.S. Bang, M. Wichmann and L. Lorentzen as well as financial support from DANSCATT.

References

1. Grønvold F, Haraldsen H, Vihovde J (2008) Acta Chem Scand 8:1927
2. Hägg G, Kindström AL (1933) Z Phys Chem B22:453
3. Finlayson DM, Greig D, Llewellyn JP, Smith T (1956) Proc Phys Soc London 69:860
4. Hsu F-C, Luo J-Y, Yeh K-W, Chen T-K, Huang T-W, Wu PM, Lee Y-C, Huang Y-L, Chu Y-Y, Yan D-C, Wu M-K (2008) Proc Nat Acad Sci USA 105:14262

5. Fang M H, Pham H M, Qian B, Liu T J, Vehstedt E K, Liu Y, Spinu L, Mao Z Q (2008) Phys Rev B 78:224503
6. Mizuguchi Y, Tomioka F, Tsuda S, Yamaguchi T, Takano Y (2009) Appl Phys Lett 94:012503
7. Mizuguchi Y, Deguchi K, Tsuda S, Yamaguchi T, Takano Y (2010) Phys Rev B 81:214510
8. Yeh K-W, Huang T-W, Huang I-L, Chen T-K, Hsu F-C, Wu P M, Lee Y-C, Chu Y-Y, Chen C-L, Luo J-Y, Yan D-C, Wu M-K (2008) Europhys Lett. 84:37002
9. Yeh KW, Hsu HC, Huang TW, Wu PM, Huang YL, Luo JY, Wu MK (2008) J Phys Soc Jpn 77(Suppl. C):19
10. Mizuguchi Y, Deguchi K, Tsuda S, Yamaguchi T, Takeya H, Kumakura H, Takano Y (2009) Appl Phys Exp 2:083004
11. Grivel J-C, Wulff AC, Zhao Y, Andersen NH, Bednarčík J, Zimmermann Mv (2011) Supercond Sci Technol 24:015007
12. Okamoto H, Tanner LE (1992) Binary alloy phase diagrams. In: Massalski T B, Okamoto H, Subramanian P R, Kacprzak L (eds) vol 2. ASM International, Materials park, p 1781
13. Abrikosov NKh, Dyul'dina KA, Zhdanova VV (1970) Khalkogenidy 2:98
14. Abrikosov N Kh, Dyul'dina KA, Zhdanova VV (1971) Chem Abstr 75:91874a
15. Ipser H, Komarek KL, Mikler H (1974) Monatshefte für Chemie 105:1322
16. Okamoto H (1992) Binary alloy phase diagrams. In: Massalski TB, Okamoto H, Subramanian PR, Kacprzak L (eds) vol 2. ASM International, Materials park, p 1769
17. Saha B, Viswanathan R, Saibara M, Darwin Albert Raj D, Balasubramanian R, Karunasagar D, Mathews CK (1985) J Nucl Mater 130:316
18. Piacente V, Scardala P, Ferro D (1992) J Alloys Comp 184:285
19. Chiba S (1955) J Phys Soc Jpn 10:837
20. Poulsen HF, Frello T, Andersen NH, Bentzon MD, Zimmermann Mv (1998) Physica C 298:265
21. Hammersley AP, Svensson SO, Hanfland M, Fitch AN, Häusermann D (1996) High Pressure Res 14:235
22. Blachnik R, Lasocka M, Walbrecht U (1983) J Sol State Chem 48:431
23. Qi YP, Zhang XP, Gao ZS, Zhang ZY, Wang L, Wang DL, Ma YW (2009) Physica C 469:717